Characterizing the mechanical deformation response of AHSS steels: A comparative study of cyclic plasticity models under monotonic and reversal loading

Toros Arda Akşen[a], Emre Esener[b], Mehmet Firat[a],*

[a] Department of Mechanical Engineering, The University of Sakarya, Sakarya, 54050, Turkey

[b] Department of Mechanical Engineering, Bilecik Seyh Edebali University, Bilecik, 11100, Turkey

(*Corresponding author: firat@sakarya.edu.tr)

ABSTRACT: This study evaluates the performance of a user-defined combined hardening modeling method for advanced high-strength steels (AHSS) under monotonic and reversal loading conditions. The plastic behavior of TWIP980 and TRIP980 AHSS sheet metals is investigated using a cyclic plasticity modeling approach. The model incorporates an isotropic von Mises yield criterion and a single-term Chaboche nonlinear kinematic hardening rule. Monotonic and reversal loading stress-strain curves are predicted and compared with experimental results. The model accurately captured the Bauschinger effect for both materials, but it needs help to effectively model the permanent softening behavior observed in TWIP980 steel. Overall, the proposed modeling method agrees well with experimental results for monotonic loading and accurately represents the Bauschinger effect and transient behavior during reversal loading. However, better improvements are needed to capture the permanent softening behavior of TWIP980 steel.

KEYWORDS: Advanced high strength steels; Cyclic plasticity; Finite element modeling; Kinematic hardening; TRIP; TWIP

RESUMEN: *Caracterización de la respuesta por deformación mecánica de los aceros AHSS: Un estudio comparativo de modelos de plasticidad cíclica bajo carga monotónica e inversa.* Este estudio evalúa el rendimiento de un método de modelado de endurecimiento combinado definido por el usuario para aceros avanzados de alta resistencia (AHSS) bajo condiciones de carga monotónica e inversa. Se investiga el comportamiento plástico de las chapas de AHSS TWIP980 y TRIP980 utilizando un enfoque de modelado de plasticidad cíclica. El modelo incorpora un criterio de fluencia de von Mises isotrópico y una regla de endurecimiento cinemático no lineal de Chaboche de un solo término. Se predicen curvas de tensión-deformación monotónicas y de carga inversa y se comparan con resultados experimentales. El modelo capta con precisión el efecto Bauschinger para ambos materiales, pero necesita ayuda para modelizar eficazmente el comportamiento de ablandamiento permanente

observado en el acero TWIP980. En general, el método de modelización propuesto concuerda bien con los resultados experimentales para la carga monótona y representa con precisión el efecto Bauschinger y el comportamiento transitorio durante la carga inversa. Sin embargo, son necesarias mejoras para captar el comportamiento de ablandamiento permanente del acero TWIP980.

ORCID ID: Toros Arda Akşen (https://orcid.org/0000-0002-7087-3216); Emre Esener (https://orcid.org/0000-0001-5854-4834); Mehmet Fırat (https://orcid.org/0000-0002-3973-4736)

1. INTRODUCTION

Advanced high-strength steels (AHSS) are extensively utilized in the automotive industry due to their high strength, good ductility, and reduced weight (Keeler *et al.*, 2017). The increased usage of AHSS in car body structures allows for weight reduction while maintaining structural integrity (Shan *et al.*, 2018). In this context, understanding the formability and mechanical behavior of AHSS steels is paramount. During sheet metal forming processes, such as bending and unbending over die/punch radii or drawing beads, the sheet materials experience cyclic loading. Accurately describing the hardening behavior during cyclic loading is crucial for reliable finite element analyses (FEA) of these processes.

The Bauschinger effect, characterized by a decrease in yield strength when the load is reversed, is a significant phenomenon observed during cyclic and reversal loading conditions (Dieter, 1988).

Traditional isotropic hardening models fail to adequately capture the Bauschinger effect, as they assume a uniform expansion of the yield surface during hardening. To accurately represent the Bauschinger effect, kinematic hardening models are employed in cyclic loading cases. These models translate the yield surface within the stress space during hardening, allowing for a more precise description of the material's behavior. The location of the yield surface is determined by the back stress tensor (α) (Banabic, 2010). Several kinematic hardening models have been proposed, including linear models by Prager (1956) and Ziegler (1959), multilinear models by Besseling (1958), Mroz (1967), Dafalias and Popov (1976), and the nonlinear models by Armstrong and Frederick (2007) and Chaboche and Rousselier (1983).

Numerous studies have investigated the definition of material behavior under cyclic loading using kinematic hardening models. Koo and Lee (2007) examined the ratcheting characteristics of modified 9Cr-1Mo steel using the Chaboche constitutive model, demonstrating the model's capability to describe cyclic behavior. Meyer *et al.* (2018) investigated kinematic hardening models for large biaxial deformations in pearlitic steel. They found that combining the Ohno and Wang (1993) model with the Burlet and Cailletaud (1986) radial evanescence term improved the prediction of material response during cyclic loading. Joo and Huh (2017) and Joo and Huh (2018) developed rate-dependent isotropic-kinematic hardening models based on Zang's isotropic-kinematic model (Zang *et al.*, 2011) to accurately describe the hardening behavior of TWIP980 and TRIP980 steels at high strain rates. Skibicki *et al.* (2022) coupled Tanaka and Chaboche hardening models to extend the usage of the Chaboche model under asynchronous loading for E235 and E335 steels. They concluded that the proposed model can be implemented for fatigue applications. Apart from the cyclic deformation of the materials, kinematic hardening is also essential for sheet metal forming operations. One of the critical issues in forming processes is the springback defect, and the kinematic hardening approach is also able to predict this behavior. Firat (2008) and Firat *et al.* (2013) successfully applied plasticity models incorporating material anisotropy and the Bauschinger effect to predict springback and formability in sheet metal forming processes. He *et al.* (2022) conducted a comparative study of kinematic hardening models of springback prediction in the U-draw bending process. They concluded that the prediction performance was affected adversely with increased grain size. Yu *et al.* (2023) employed a nonlinear kinematic hardening model to predict the springback behavior of AHSS steels in the U-draw bending process under different blank holder forces and friction coefficients. They obtained accurate results for predicting the Bauschinger effect and springback profile of AHSS steels. Besides, kinematic hardening can also be utilized in cup drawing processes to predict earing defects. Aksen and Firat (2023) also implemented an anisotropic yield criterion in conjunction with the isotropic hardening model and combined isotropic-Armstrong-Frederic kinematic hardening model separately to capture the earing defect of AA6016-T4 alloy in a cup drawing process. It was seen that the earing prediction performance was noticeably increased when the combined isotropic-kinematic hardening model was assumed.

This study investigates the plastic behavior of TWIP980 and TRIP980 steels, representative of AHSS, under monotonic and reversal loading conditions. TRIP steel is a first-generation AHSS, while TWIP steel is a second-generation. In the structure of the TRIP steels,

ferrite, martensite, residual austenite, and bainite are present. During the deformation, the residual austenite transforms to the martensite. Thus, the hardening rate is increased, and high ductility and strength are ensured. This type of transformation is also called the TRIP effect in the literature (Jacques *et al.*, 2001; Muransky *et al.*, 2008; Fu *et al.*, 2014).

On the other hand, TWIP steels contain a high ratio of manganese to maintain the austenitic structure. This structure ensures the twinning mode of the deformation along with the dislocations. Accordingly, the hardening rate is increased stemming from both twinning and dislocation coalescence, which postpones the localization of the deformation (Grassel *et al.*, 2000; Prakash *et al.*, 2008).

A combined hardening model comprises an isotropic von Mises yield criterion and a single-term Chaboche nonlinear kinematic hardening rule. The model is implemented in a commercial finite element code, and FE analyses of tension and tension-compression tests are performed. The predicted stress-strain curves under monotonic and reversal loading conditions are compared with experimental results to evaluate the model's predictive capability.

The accuracy of the presented cyclic plasticity model is assessed by examining the agreement between the predicted and experimental stress-strain curves. The outcomes of this research contribute to a better understanding of the mechanical behavior of AHSS steels under different loading conditions and provide insights for improving the modeling of their response.

This study contains 5 sections. In section 2, the governing equations of the cyclic plasticity modeling and the construction of the FE model were presented. Section 3 summarizes the prediction results of monotonic and cyclic loading conditions. In section 4, the results, which were compared with the experimental outcomes, were discussed and the conclusions were summarized in section 5.

2. MATERIALS AND METHODS

In this section, relevant information related to plasticity modeling and finite element modeling was given. In this study, TRIP980 and TWIP980 steels were selected to investigate the cyclic response of the material. The TRIP steel contains C (0.21%), Mn (1.5%), Si (0.24%), Al (1.6%), with iron balance, while the TWIP steels contain high Mn content (16%). Apart from the Mn, these steels contain high C content of 0.66%, Si (0.035%), P (0.01%), with iron balance.

2.1. Cyclic plasticity modeling

The strain increment can be decomposed into elastic and plastic components (Yildiz and Kirli, 2004),

$$d\varepsilon = d\varepsilon_e + d\varepsilon_p \qquad (1)$$

where the elastic component consists of deviatoric and hydrostatic components, and the plastic component is entirely deviatoric.

$$d\varepsilon_e = de_e + d\varepsilon_m I \qquad (2)$$

Here, I denotes the Kronecker delta and ε_m represents the mean strain. The Cauchy stress tensor can be divided into elastic and plastic parts as well.

$$d\sigma = dS + d\sigma_m I \qquad (3)$$

The deviatoric stress increment can be found by the deviatoric elastic strain increment as in Eq. (4).

$$dS = 2Gde_e \qquad (4)$$

where, G refers to as shear modulus. This study employs a cyclic plasticity model, incorporating an isotropic von Mises yield criterion and a single-term Chaboche nonlinear kinematic hardening rule (Chaboche and Rousselier, 1983). The yield function is dictated by the von Mises criterion that is given in Eq. (5).

$$f = \|S - \alpha\| - \sqrt{\frac{2}{3}}\sigma_0 \qquad (5)$$

The Chaboche model describes the evolution of the yield surface during plastic deformation using a back-stress tensor (α) and includes both linear and nonlinear components (Pajand and Sinaie, 2009; Paul *et al.*, 2010).

$$d\alpha = \frac{2}{3}Cd\varepsilon_p - \gamma\alpha dp \qquad (6)$$

In Eq. (6), C and γ are the material parameters controlling the translation of the yield locus. The first term of this expression is the linear part of the backstress, while the second term refers to the fading memory term that provides the saturation of the backstress at C/γ (Paul *et al.*, 2010). dp represents the equivalent plastic strain and can be expressed as follows.

$$dp = \sqrt{\frac{2}{3}d\varepsilon_p.d\varepsilon_p} \qquad (7)$$

The relationship between the plastic strain increment and the stresses follows the normality rule, based on the flow tensor usual to the yield stress at the current stress point.

$$\varepsilon_p = \frac{1}{h}(dS:n) \qquad (8)$$

Here, n denotes the normal direction of the flow tensor, and a hardening modulus (h) is included to satisfy the consistency condition during plastic flow. The stress state should satisfy the consistency condition that is governed by Eq. (9).

$$df = dS:n - d\alpha:n = 0 \qquad (9)$$

2.2. Finite element model of tension-compression test

A tension-compression test is conducted using TWIP980 and TRIP980 steels to validate the proposed cyclic plasticity model. The test data is obtained from previous work (Joo and Huh, 2018) and the thickness was considered as 1 mm. The dimensions of the specimen are shown in Fig. 1.
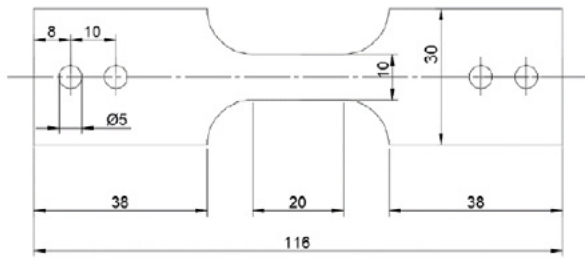

FIGURE 1. Dimensions of test specimen (Joo and Huh, 2018)

The finite element model of the specimen is created using an implicit finite element code (MSC Marc). The reduced region of the sample is discretized with fine meshes to capture stress-strain data accurately. Eight-node fully integrated hexahedral elements are utilized (Marc (2018a) and Marc (2018b)) with the dimensions of the solid element set as 0.86x1x1 mm (Fig. 2).
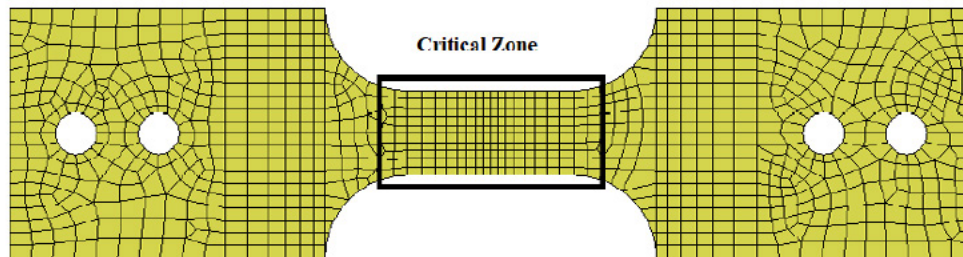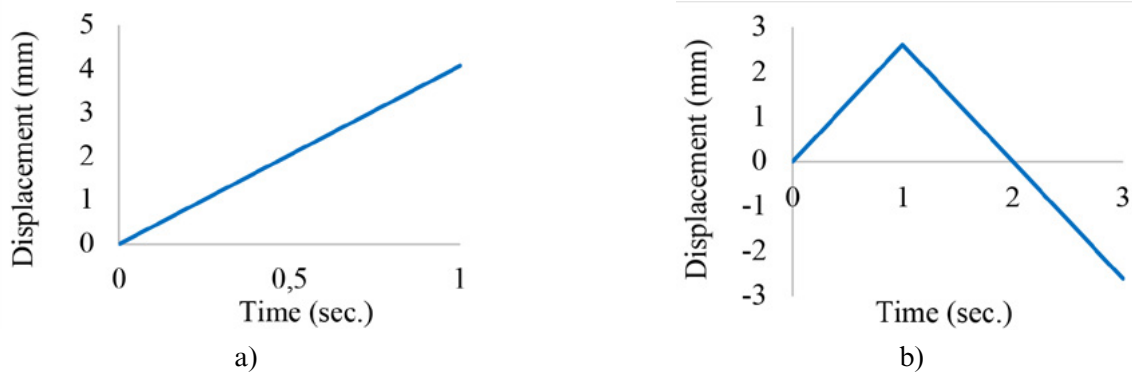
A spring-loaded clamping device is incorporated to prevent buckling during the compression stage. The specimen is fixed at one end, and displacement is applied to the other. The loading history for both monotonic and reversal loading conditions is illustrated in Fig. 3.

The isotropic hardening parameters for TWIP980 and TRIP980 steels are determined using the Swift hardening law (Eq. (10)).

$$\sigma_{true} = K(\varepsilon_0 + \varepsilon_p)^p \qquad (10)$$

The Swift parameters are calibrated to fit the experimental flow curve. To this end, the MATLAB Curve Fitting Tool (CFTool) was utilized, and the Levenberg-Marquardt algorithm (Sapna *et al.*, 2012) embedded into the software was adopted. Here, p represents the hardening exponent related to the slope of the flow curve, while K and ε_p represent the strength coefficient and the plastic strain values, respectively. Apart from them, the yield stress was dictated by the parameter ε_0. Both materials' experimental and Swift hardening curves are compared to validate the chosen parameters. The flow curves were given in Fig. 4 and the hardening parameters provided in Table 1.

The kinematic hardening part was characterized by the single-term Chaboche model that is given in Eq. (11) and Table 2 presents the kinematic hardening parameters.

FIGURE 2. FE model of the specimen

FIGURE 3. Loading history for a) Monotonic, b) Reversal loading

TABLE 1. Hardening curve parameters of the steels

TWIP980	Parameter	TRIP980
1685	K (MPa)	1700
0.26	n	0.19
0.0065	ε_0	0.0024

TABLE 2. Kinematic hardening parameters of the steels

Parameter	TWIP980	TRIP980
C (MPa)	10000	16668
γ	55.56	55.56

a)

b)
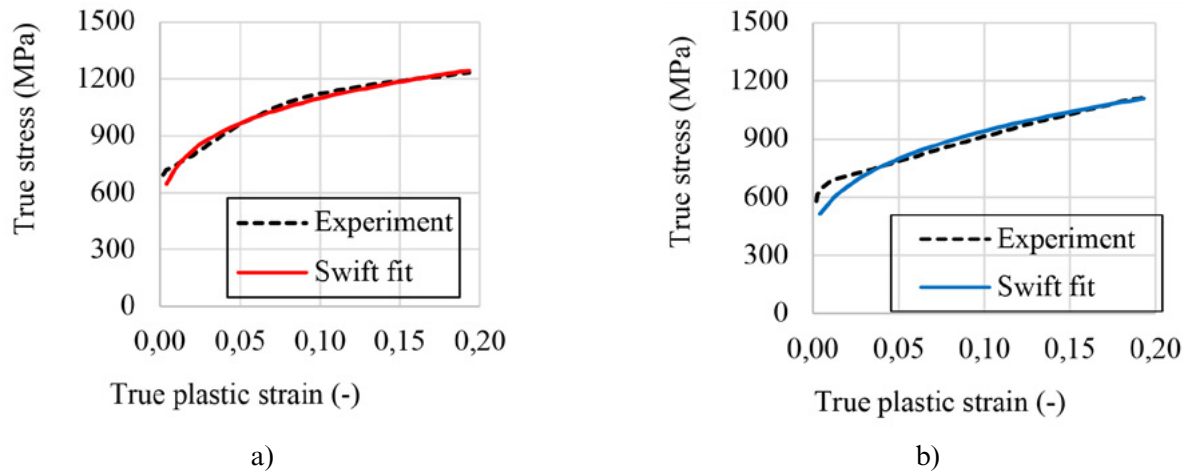
FIGURE 4. The hardening curves of a) TRIP980, b) TWIP980

$$\alpha = \frac{C}{\gamma}(1 - e^{-\gamma \varepsilon_p}) \qquad (11)$$

Eq. (11) is the integrated form of Eq. (6). The parameters C and γ are the material parameters controlling the translation of the yield locus. C/γ is the threshold at which the back stress saturates. The back stress curves were constructed based on the calibrated parameters and these curves are presented in Fig. 5.
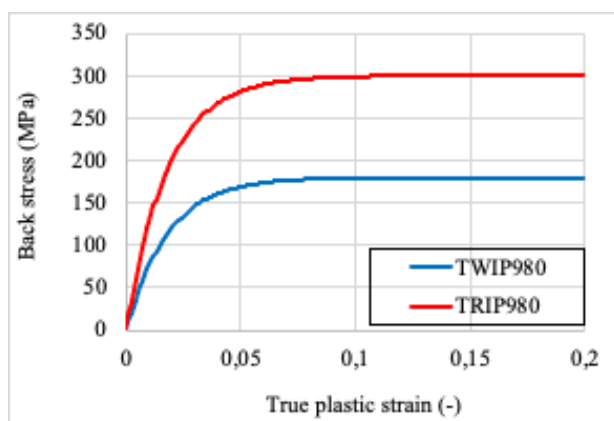
FIGURE 5. Back stress curves of the steels

The proposed cyclic plasticity model is implemented in the commercial finite element code with the deter-mined isotropic and kinematic hardening parameters. The stress-strain curves under monotonic and reversal loading conditions are predicted and compared with the experimental results.

3. RESULTS

After determining the hardening parameters, finite element analyses evaluate the stress-strain response of TWIP980 and TRIP980 steels under monotonic and reversal loading conditions. The predicted stress-strain curves are compared with experimental data (Fig. 6).

Figure 6 compares the predicted and experimental hardening curves for monotonic loading conditions. It is observed that the predicted stress-strain curves ac-curately align with the experimental results for both TRIP980 and TWIP980 steels. Figure 7 compares the predicted and experimental hardening curves for rever-sal loading conditions.

The model successfully captures the Bauschinger effect, with a decrease in yield strength when the load is reversed, for both materials. The predicted yield strengths in compression for both steels were close to each other and approximately 600 MPa. These values were found compatible with the experimental behavior. 1100 MPa and 920 MPa are the approximate thresholds reached at the end of the loading sequence for TRIP980 and TWIP980 steels, respectively. These values were also the yield stresses if these steels were loaded in the same direction (tension). However, when these steels
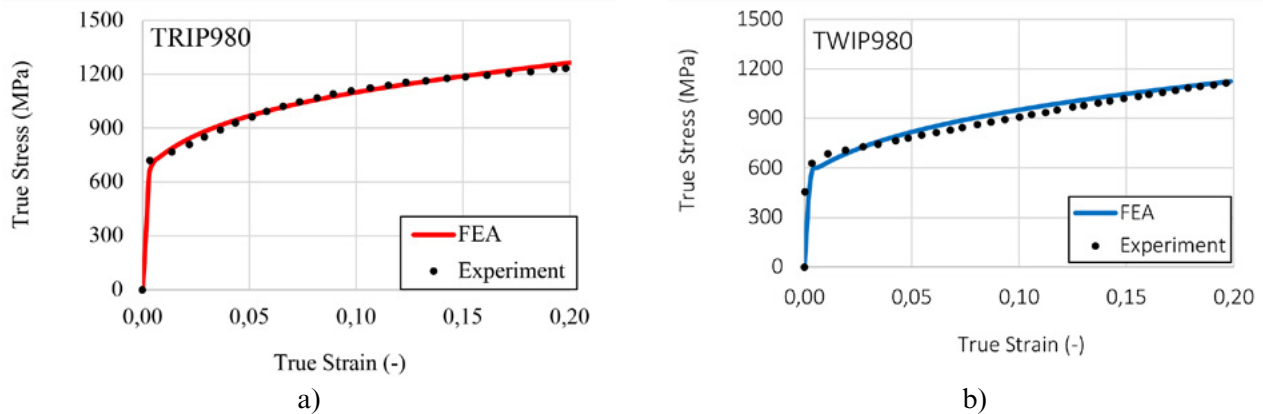
FIGURE 6. The predicted and experimental stress-strain responses for monotonic loading of a) TRIP980, b) TWIP980 steels
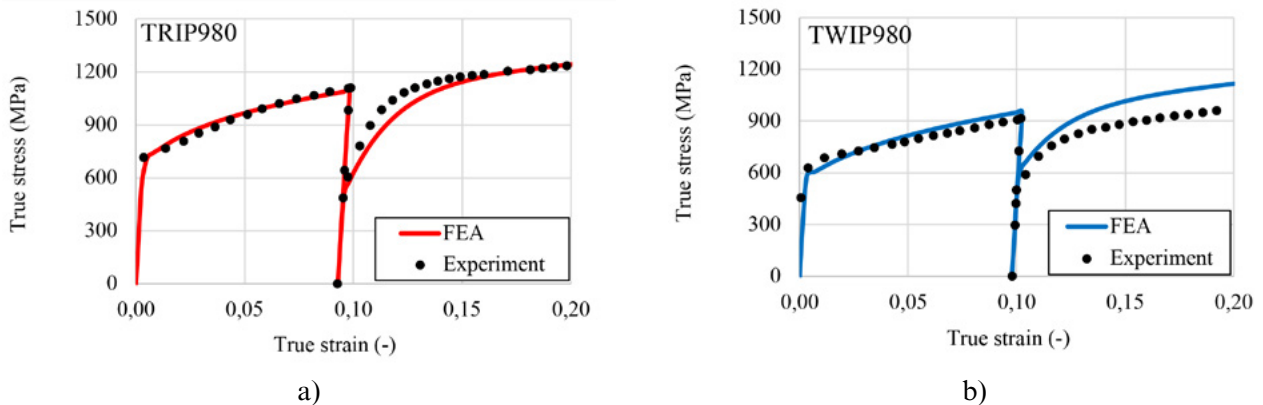

FIGURE 7. The predicted and experimental stress-strain responses for reversal loading of a) TRIP980, b) TWIP980 steels

were subsequently loaded in compression, the change in TRIP980 steel was found to be more apparent. This situation shows that the Bauschinger effect was more dominant for TRIP980 steel when compared to the TWIP980 steel. The stress-strain behavior of TRIP980 steel is well-predicted by the model, while a minor deviation is observed for TWIP980 steel. This discrepancy can be attributed to the permanent softening behavior exhibited by TWIP980 steel, resulting from the dissolution of the cell walls of dislocations (Zang *et al.*, 2011). Based on Armstrong-Frederick-type unified models, the current model cannot fully represent this behavior.

4. DISCUSSION

This work employs a user-defined combined hardening model to characterize the stress-strain response of TWIP980 and TRIP980 steels under monotonic and reversal loading conditions. The model incorporates an isotropic von Mises yield criterion and a single-term Chaboche nonlinear kinematic hardening rule. The predicted stress-strain curves demonstrate good agree-

ment with experimental results for monotonic loading conditions, indicating the accuracy of the proposed model.

Furthermore, the model effectively captures the Bauschinger effect and transient behavior during reversal loading for both materials. Zang *et al.* (2011) studied the springback response in U-draw bending for an aluminum alloy. Since the kinematic hardening rule is significant for springback prediction, they utilized and calibrated a unified hardening model. They observed that the Armstrong-Frederic type hardening models can capture the Bauschinger effect and transient behavior. Çaylak *et al.* (2022) also utilized the Armstrong-Frederic type hardening model to characterize the deformation behavior of oxygen-free high thermal conductivity copper material under combined tensile and cyclic bending loads. They also observed similar outcomes. In this work, a minor deviation is observed in the stress-strain response of TWIP980 steel, attributed to its permanent softening behavior. Similar results were also recorded in the study of Fu *et al.* (2016). They adopted nonlinear kinematic hardening models and observed for the TWIP980 steel that the numeri-

cal results deviated from the experimental reciprocals. The inability of the Armstrong-Frederick type unified models to represent this behavior highlights the need for further improvements in modeling the permanent softening observed in TWIP980 steel.

The demonstrated combined hardening model provides a practical and user-friendly approach to characterize the stress-strain response of AHSS steels under different loading conditions. The model successfully predicts the material behavior of TWIP980 and TRIP980 steels. However, modifications or alternative modeling approaches may be necessary to enhance its capability and fully capture the permanent softening behavior (Zang *et al.* (2011). The findings of this study contribute to a better understanding of the mechanical behavior of AHSS steels and provide insights for further advancements in modeling their response under monotonic and reversal loading conditions.

5. SUMMARY AND CONCLUSIONS

This study evaluated the performance of a user-defined combined hardening modeling method for advanced high-strength steels (AHSS) under monotonic and reversal loading conditions. The plastic behavior of TWIP980 and TRIP980 steels was investigated using a cyclic plasticity modeling approach, incorporating an isotropic von Mises yield criterion and a single-term Chaboche nonlinear kinematic hardening rule.

The results of the study demonstrate the following conclusions:
- The proposed combined hardening model accurately predicts the stress-strain response under monotonic loading conditions for TWIP980 and TRIP980 steels, showing good agreement with experimental results.
- The model successfully captures the Bauschinger effect and transient behavior observed during reversal loading for both materials, indicating its ability to represent the cyclic behavior.
- However, the model exhibits a minor deviation in predicting the stress-strain behavior of TWIP980 steel during reversal loading. This discrepancy is attributed to the permanent softening behavior of TWIP980 steel, which the current model, based on Armstrong-Frederick-type unified models, cannot fully capture.
- The user-defined combined hardening model presented in this study provides a practical and user-friendly approach to characterize the stress-strain response of AHSS steels under monotonic and reversal loading conditions.

The findings of this study contribute to a better understanding of the mechanical behavior of TWIP980 and TRIP980 steels under different loading conditions. The model's accuracy in capturing the Bauschinger effect and transient behavior demonstrates its potential for predicting the material response in AHSS applica-

tions. However, further improvements or alternative modeling approaches are required to effectively represent the permanent softening behavior observed in TWIP980 steel.

Future research efforts should focus on enhancing the modeling capabilities to capture the complex behavior of AHSS steels, including their permanent softening behavior. This will facilitate more accurate predictions of the material response and enable the reliable simulation of AHSS components in various industrial applications.

REFERENCES

Akşen, T.A., Firat, M. (2023). Effect of the yield surface evolution on the earing defect prediction. *Rev. Metal.* 59 (1), e235. https://doi.org/10.3989/revmetalm.235.

Armstrong, P.J., Frederic, C.O. (2007). A mathematical representation of the multiaxial Bauschinger effect. *Mater. High Temp.* 24 (1), 1-26. https://doi.org/10.1179/096034007X207589.

Banabic, D. (2010). *Sheet Metal Forming Processes – Constitutive Modelling and Numerical Simulation*. Berlin, Germany, Springer.

Besseling, J.F. (1958). A theory of plastic and creep deformations of an initially isotropic material Showing Anisotropic Strain-in-Hardening, Creep Recovery, and Secondary Creep. *J. Appl. Mech.* 25 (4), 529-536. https://doi.org/10.1115/1.4011867.

Burlet, H., Cailletaud, G. (1986). Numerical techniques for cyclic plasticity at variable temperature. *Eng. Comput.* 3 (2), 143-153. https://doi.org/10.1108/eb023652.

Chaboche, J.L., Rousselier, G. (1983). On the plastic and visco-plastic constitutive equations – Part I: Rules developed with internal variable concept. *J. Press. Vessel Technol.* 105 (2), 153-158. https://doi.org/10.1115/1.3264257.

Çaylak, M., Akşen, T.A., Fırat, M. (2022). Evaluating the effectiveness of combined hardening models to determine the behavior of a plate with a hole under combined loadings. *Eur. Mech. Sci.* 6 (2), 97-104. https://doi.org/10.26701/ems.1051057.

Dafalias, Y.F., Popov, E.F. (1976). Plastic internal variables formalism of cyclic plasticity. *J. Appl. Mech.* 43 (4), 645-651. https://doi.org/10.1115/1.3423948.

Dieter, G.E. (1988). *Mechanical Metallurgy*. SI metric ed. New York, USA, Mc-Graw Hill Book Company.

Firat, M. (2008). A numerical analysis of sheet metal formability for automotive stamping applications. *Comput. Mater. Sci.* 43 (4), 802-811. https://doi.org/10.1016/j.commatsci.2008.01.068.

Firat, M., Karadeniz, E., Yenice, M., Kaya, M. (2013). Improving the accuracy of stamping analyses including springback deformations. *J. Mater. Eng. Perform.* 22, 332-337. https://doi.org/10.1007/s11665-012-0257-5.

Fu, B., Yang, W.Y., Wang, Y.D., Li, L.F., Sun, Z.Q., Ren, Y. (2014). Micromechanical behavior of TRIP-assisted multiphase steels studied with in situ high-energy X-ray diffraction. *Acta Mater.* 76, 342–354. https://doi.org/10.1016/j.actamat.2014.05.029.

Fu, J., Barlat, F., Kim, J.H., Pierron, F. (2016). Identification of nonlinear kinematic hardening constitutive model parameters using the virtual fields method for advanced high strength steels. *Int. J. Solids Struct.* 102-103, 30 – 43. https://doi.org/10.1016/j.ijsolstr.2016.10.020.

Grassel, O., Krüger, L., Frommeyer, G., Meyer, L.W. (2000). High strength Fe-Mn-(Al, Si) TRIP/TWIP steels development – properties – applications. *Int. J. Plast.* 16 (10-11), 1391-1409. https://doi.org/10.1016/S0749-6419(00)00015-2.

He, W., Meng, B., Song, B., Wan, M. (2022). Grain size effect on cyclic deformation behavior and springback prediction Ni-based superalloy foil. *Trans. Nonferrous Metal. Soc. China* 32 (4), 1188 – 1204. https://doi.org/10.1016/S1003-6326(22)65866-7.

Jacques, P.J., Delannay, F., Ladriere, J. (2001). On the influence of interactions between phases on the mechanical stability of retained austenite in transformation-induced plasticity multiphase steels. *Metal. Mater. Trans. A* 32, 2759–2768. https://doi.org/10.1007/s11661-001-1027-4.

Joo, G., Huh, H. (2017). Modeling of rate-dependent hardening behaviors of the TWIP980 steel sheet in tension and compression. *Procedia Eng.* 207, 143-148. https://doi.org/10.1016/j.proeng.2017.10.752.

Joo, G., Huh, H. (2018). Rate-dependent isotropic-kinematic hardening model in tension-compression of TRIP and TWIP steel sheets. *Int. J. Mech. Sci.* 146-147, 432-444. https://doi.org/10.1016/j.ijmecsci.2017.08.055.

Keeler, S., Kimchi, M., Mooney, P.J. (2017). *Advanced High-Strength Steels Application Guidelines.* Version 6.0, World Auto Steel. https://www.worldautosteel.org/download_files/AHSS%20Guidelines%20V6/00_AHSSGuidelines_V6_20170430.pdf

Koo, G.H., Lee, J.H. (2007). Investigation of ratcheting characteristics of modified 9Cr-1Mo steel by using the Chaboche constitutive model. *Int. J. Press. Vessel Pip.* 84 (5), 284-292. https://doi.org/10.1016/j.ijpvp.2006.12.002.

Marc (2018a). Volume A: Theory and User Information.

Marc (2018b). Volume B: Element library

Meyer, K.A., Ekh, M., Ahlström, J. (2018). Modeling of kinematic hardening at large biaxial deformations in pearlitic steel. *Int. J. Solids Struct.* 130, 122-132. https://doi.org/10.1016/j.ijsolstr.2017.10.007.

Mróz, Z. (1967). On the description of anisotropic work hardening. *J. Mech. Phys. Solids.* 15 (3), 163-175. https://doi.org/10.1016/0022-5096(67)90030-0.

Muransky, O., Sittner, P., Zrník, J., Oliver, E.C. (2008). *In situ* neutron diffraction investigation of the collaborative deformation-transformation mechanism in TRIP assisted steels at room and elevated temperatures. *Acta Mater.* 56 (14), 3367–3379. https://doi.org/10.1016/j.actamat.2008.03.026.

Ohno, N., Wang, J.-D. (1993). Kinematic hardening rules with critical state of dynamic recovery. Part I: formulation and basic features for ratchetting behavior. *Int. J. Plast.* 9 (3), 375-390. https://doi.org/10.1016/0749-6419(93)90042-O.

Pajand, M.R., Sinaie, S. (2009). On the calibration of Chaboche model and modified hardening rule for uniaxial ratcheting prediction. *Int. J. Solids Struct.* 46 (16), 3009-3017. https://doi.org/10.1016/j.ijsolstr.2009.04.002.

Paul, S.K., Sivaprasad, S., Dhar, S., Tarafder, M., Tarafder, S. (2010). Simulation of cyclic plastic deformation response in SA333 C-Mn steel by a kinematic hardening model. *Comput. Mater. Sci.* 48 (3), 662-671. https://doi.org/10.1016/j.commatsci.2010.02.037.

Prager, W. (1956). A new method of analyzing stresses and strains in work hardening plastic solids. *ASME J. Appl. Mech.* 23 (4), 493-496. https://doi.org/10.1115/1.4011389.

Prakash, A., Hochrainer, H., Reisacher, E., Riedel, H. (2008). Twinning models in self-consistent texture simulations of TWIP steels. *Steel Res. Int.* 79 (8), 645-645. https://doi.org/10.1002/srin.200806178.

Sapna, S., Tamilarasi, A., Kumar, M.P. (2012). Backpropagation learning algorithm based on Levenberg Marquardt algorithm. Comput. *Sci. Inf. Technol.,* pp. 393-398. https://doi.org/10.5121/csit.2012.2438.

Shan, T.K., Li, S.H., Zhang, W.G., Xu, Z.G. (2018). Prediction of martensitic transformation and deformation behavior in the TRIP steel sheet forming. *Mater. Des.* 29 (9), 1810-1816. https://doi.org/10.1016/j.matdes.2008.03.023.

Skibicki, D., Pejkowski, L., Karolczuk, A., Seyda, J. (2022). Verification of the Tanaka non-proportional isotropic cyclic hardening model under asynchronous loading. *Int. J. Solids Struct.* 254-255, 111896. https://doi.org/10.1016/j.ijsolstr.2022.111896.

Yıldız, H., Kırlı, O. (2004). Non-linear finite element modeling of deep drawing process. *Pamukkale University J. Eng. Sci.* 10 (3), 317-326.

Yu, K., Choi, H., Ha, J., Yoon, J.W. (2023). Bauschinger effect calibration by the different types of loading/reverse loading tests for springback prediction in sheet metal forming. *Int. J. Mater. Form.* 16, 16. https://doi.org/10.1007/s12289-023-01738-3.

Zang, S.L., Guo, C., Thuillier, S., Lee, M.G. (2011). A model of one-surface cyclic plasticity and its application to springback prediction. *Int. J. Mech. Sci.* 53 (6), 425-435. https://doi.org/10.1016/j.ijmecsci.2011.03.005.

Ziegler, H.A. (1959). A modification of Prager's hardening rule. *Q. Appl. Math.* 17 (1), pp. 55-65.